

# Wireless bioresorbable electronic system enables sustained nonpharmacological neuroregenerative therapy

Jahyun Koo<sup>1,2,16</sup>, Matthew R. MacEwan<sup>3,4,16</sup>, Seung-Kyun Kang<sup>5,6,16</sup>, Sang Min Won<sup>7</sup>, Manu Stephen<sup>3</sup>, Paul Gamble<sup>3</sup>, Zhaoqian Xie<sup>2,8</sup>, Ying Yan<sup>3</sup>, Yu-Yu Chen<sup>7</sup>, Jiho Shin<sup>7</sup>, Nathan Birenbaum<sup>3,4</sup>, Sangjin Chung<sup>7</sup>, Sung Bong Kim<sup>7</sup>, Jawad Khalifeh<sup>3</sup>, Daniel V. Harburg<sup>7</sup>, Kelsey Bean<sup>3</sup>, Michael Paskett<sup>3</sup>, Jeonghyun Kim<sup>9</sup>, Zohny S. Zohny<sup>3</sup>, Seung Min Lee<sup>1,2</sup>, Ruoyao Zhang<sup>7</sup>, Kaijing Luo<sup>2,8</sup>, Bowen Ji<sup>2,8</sup>, Anthony Banks<sup>2,7</sup>, Hyuck Mo Lee<sup>10</sup>, Younggang Huang<sup>1,2,8</sup>, Wilson Z. Ray<sup>3,4\*</sup> and John A. Rogers<sup>1,2,7,8,11,12,13,14,15\*</sup>

**Peripheral nerve injuries represent a significant problem in public health, constituting 2–5% of all trauma cases<sup>1</sup>. For severe nerve injuries, even advanced forms of clinical intervention often lead to incomplete and unsatisfactory motor and/or sensory function<sup>2</sup>. Numerous studies report the potential of pharmacological approaches (for example, growth factors, immunosuppressants) to accelerate and enhance nerve regeneration in rodent models<sup>3–10</sup>. Unfortunately, few have had a positive impact in clinical practice. Direct intraoperative electrical stimulation of injured nerve tissue proximal to the site of repair has been demonstrated to enhance and accelerate functional recovery<sup>11,12</sup>, suggesting a novel nonpharmacological, bioelectric form of therapy that could complement existing surgical approaches. A significant limitation of this technique is that existing protocols are constrained to intraoperative use and limited therapeutic benefits<sup>13</sup>. Herein we introduce (i) a platform for wireless, programmable electrical peripheral nerve stimulation, built with a collection of circuit elements and substrates that are entirely bioresorbable and biocompatible, and (ii) the first reported demonstration of enhanced neuroregeneration and functional recovery in rodent models as a result of multiple episodes of electrical stimulation of injured nervous tissue.**

To overcome the limitations of existing surgical approaches to deliver electrical stimulation, we have developed a platform to enable electrical stimulation of injured nerves that extends beyond the intraoperative period to facilitate nerve regeneration (Supplementary Figs. 1 and 2). Fig. 1a highlights the design

features and key materials of the enabling technology—a bioresorbable, implantable wireless stimulator that combines a radio frequency power harvester (left) and an electrical interface to a targeted peripheral nerve (right). The harvester consists of a loop antenna with a bilayer, dual-coil configuration (Mg, ~50 μm thick) with a poly (lactic-co-glycolic acid) (PLGA) dielectric interlayer, a radio frequency diode based on a doped silicon nanomembrane (~320 nm thick) with electrodes of Mg (~300 nm thick), and a parallel plate capacitor that uses Mg conducting planes (~50 μm thick) above and below a dielectric of silicon dioxide (SiO<sub>2</sub>, ~600 nm thick). Here, the exposed electrode (1.7 mm<sup>2</sup>) encircles the nerve (Fig. 1a, right inset) as part of a tubular structure of hot-pressed PLGA (~30 μm thick) with a slit along the length of one side to facilitate surgical application. A biodegradable metal strip (50 μm thick of Mg or 10 μm thick of Mo with a 340 μm width) embedded in the PLGA with an opening at the end serves as an electrical connection, through a deposited layer of Mg (~2.5 μm thick), to deliver electrical stimuli from the receiver antenna to the tissue. Careful examination of the nerve and the nerve cuff before and after 8 weeks of implantation revealed no sign of nerve damage or compressive axonopathy (Supplementary Fig. 3)<sup>14–16</sup>. Fig. 1b shows a photograph of the complete system (width: ~10 mm; length: ~40 mm; thickness: ~200 μm; weight: 150 mg). Fig. 1c presents an outline of the operational scheme. Modulation of radio frequency power supplied to a transmission antenna placed near the harvester delivers cathodic, monophasic electrical impulses (duration: 200 μs; threshold voltage: 100–300 mV) to the interfaced region of the nerve. This inductive coupling power transfer scheme has been employed effectively in

<sup>1</sup>Center for Bio-Integrated Electronics, Northwestern University, Evanston, IL, USA. <sup>2</sup>Department of Materials Science Engineering, Northwestern University, Evanston, IL, USA. <sup>3</sup>Department of Neurological Surgery, Washington University School of Medicine, St Louis, MO, USA.

<sup>4</sup>Department of Biomedical Engineering, Washington University, St Louis, MO, USA. <sup>5</sup>Department of Bio and Brain Engineering, Korea Advanced Institute of Science & Technology, Daejeon, Republic of Korea. <sup>6</sup>KAIST Institute for Health Science and Technology, Korea Advanced Institute of Science & Technology, Daejeon, Republic of Korea. <sup>7</sup>Frederick Seitz Materials Research Laboratory, University of Illinois at Urbana-Champaign, Urbana, IL, USA.

<sup>8</sup>Department of Civil and Environmental Engineering, Northwestern University, Evanston, IL, USA. <sup>9</sup>Department of Electronics Convergence Engineering, Kwangju University, Nowon-gu, Seoul, Republic of Korea. <sup>10</sup>Department of Materials Science and Engineering, Korea Advanced Institute of Science & Technology, Daejeon, Republic of Korea. <sup>11</sup>Departments of Electrical Engineering, Computer Science, Chemistry and Biomedical Engineering, Northwestern University, Evanston, IL, USA. <sup>12</sup>Simpson Querrey Institute for Nano/biotechnology, Northwestern University, Evanston, IL, USA. <sup>13</sup>McCormick School of Engineering, Northwestern University, Evanston, IL, USA. <sup>14</sup>Feinberg School of Medicine, Northwestern University, Evanston, IL, USA. <sup>15</sup>Department of Neurological Surgery, Northwestern University, Evanston, IL, USA. <sup>16</sup>These authors contributed equally: Jahyun Koo, Matthew R. MacEwan, Seung-Kyun Kang. \*e-mail: [rayz@wudosis.wustl.edu](mailto:rayz@wudosis.wustl.edu); [jrogers@northwestern.edu](mailto:jrogers@northwestern.edu)

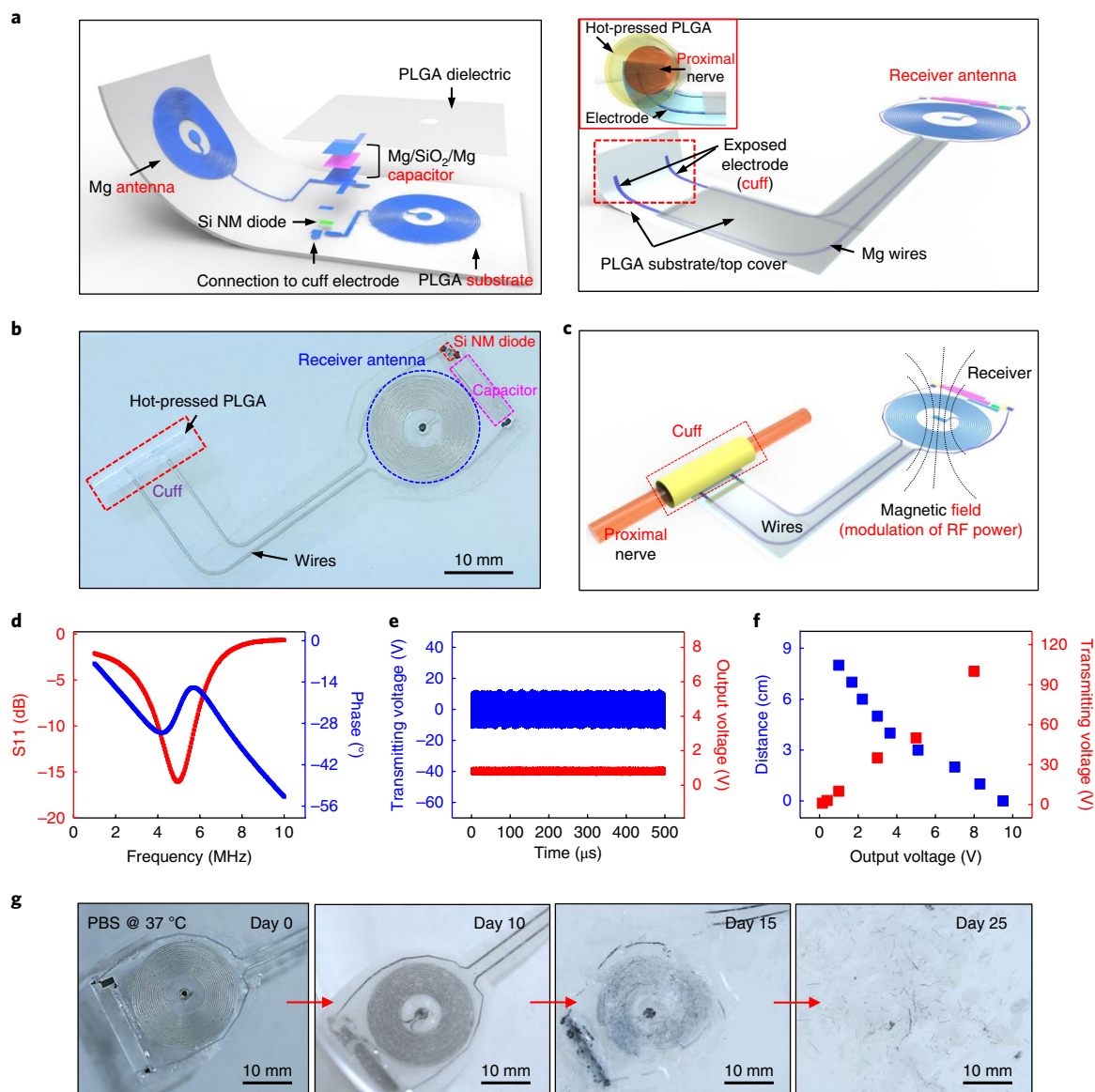


**Fig. 1 | Bioresorbable, wireless electrical stimulator as an electronic neuroregenerative medical device. a**, Schematic illustration of the device design. The electronic component is a wireless receiver that acts as a radio frequency power harvester, built with an inductor (Mg coil, 50  $\mu\text{m}$  thick), a radio frequency diode (Si nanomembrane active layer, 320 nm thick; Mg electrodes, 300 nm thick), a Mg/SiO<sub>2</sub>/Mg capacitor (50  $\mu\text{m}$ /600 nm/50  $\mu\text{m}$  thick), and a PLGA substrate (30  $\mu\text{m}$  thick) interconnected with Mg deposited by sputtering (2.5  $\mu\text{m}$ ) (left). Folding the constructed system in half yields a compact device with a double-coil inductor. The electrode and cuff interface for nerve stimulation is shown on the right. This part of the system includes metal electrodes (Mo, 10  $\mu\text{m}$  thick, or Mg, 50  $\mu\text{m}$  thick with a 340  $\mu\text{m}$  width) embedded in a PLGA substrate (30  $\mu\text{m}$  thick) with an encapsulating overcoat of PLGA (30  $\mu\text{m}$  thick). Rolling the end of the system into a cylinder creates a cuff with exposed electrodes at the ends as an interface to the nerve. **b**, Image of a completed device. **c**, Schematic of wireless operation, including the nerve interface. **d**, Radio frequency behavior of the stimulator (red,  $S_{11}$ ; blue, phase). The resonance frequency is ~5 MHz, selected to allow magnetic coupling in a frequency regime with little parasitic absorption by biological tissues ( $n=3$  independent samples). **e**, Example output waveform (stimulator, red) wirelessly generated by an alternating current (sine wave) applied to the transmission coil (transmitter, blue;  $n=3$  independent samples). **f**, Output voltage as a function of distance between the harvester and transmitter (blue), and the voltage applied to the transmitter (red). 1 k $\Omega$  load used.  $n=3$  independent samples. **g**, Images of dissolution of a bioresorbable wireless stimulator associated with immersion in PBS (pH=7.4) at 37  $^{\circ}\text{C}$ .

the field of cochlear implants across an interposing layer of skin and subcutaneous tissue<sup>17,18</sup>.

Fig. 1d,f summarize the electrical performance characteristics of the bioresorbable wireless stimulator. Radio frequency power transfer relies on magnetic coupling (Fig. 1d, ~5 MHz), thereby avoiding the losses associated with absorption by biofluids<sup>19</sup>. Fig. 1e highlights the monophasic output (1 V) generated by the harvester for continuous and pulsed radio frequency

power (~11 V<sub>pp</sub> at an 80 mm coupling distance) applied to the transmission antenna. As in Fig. 1f, for distances of up to 80 mm, voltages of 100–300 mV can be generated at the nerve, corresponding to the threshold voltages for inducing nerve activation (Supplementary Fig. 4 and Supplementary Video 1). Increased depths of stimulation can be achieved by increasing the power (Supplementary Fig. 5). These parameters suggest that the device should operate successfully not only in large animal models<sup>20</sup> but

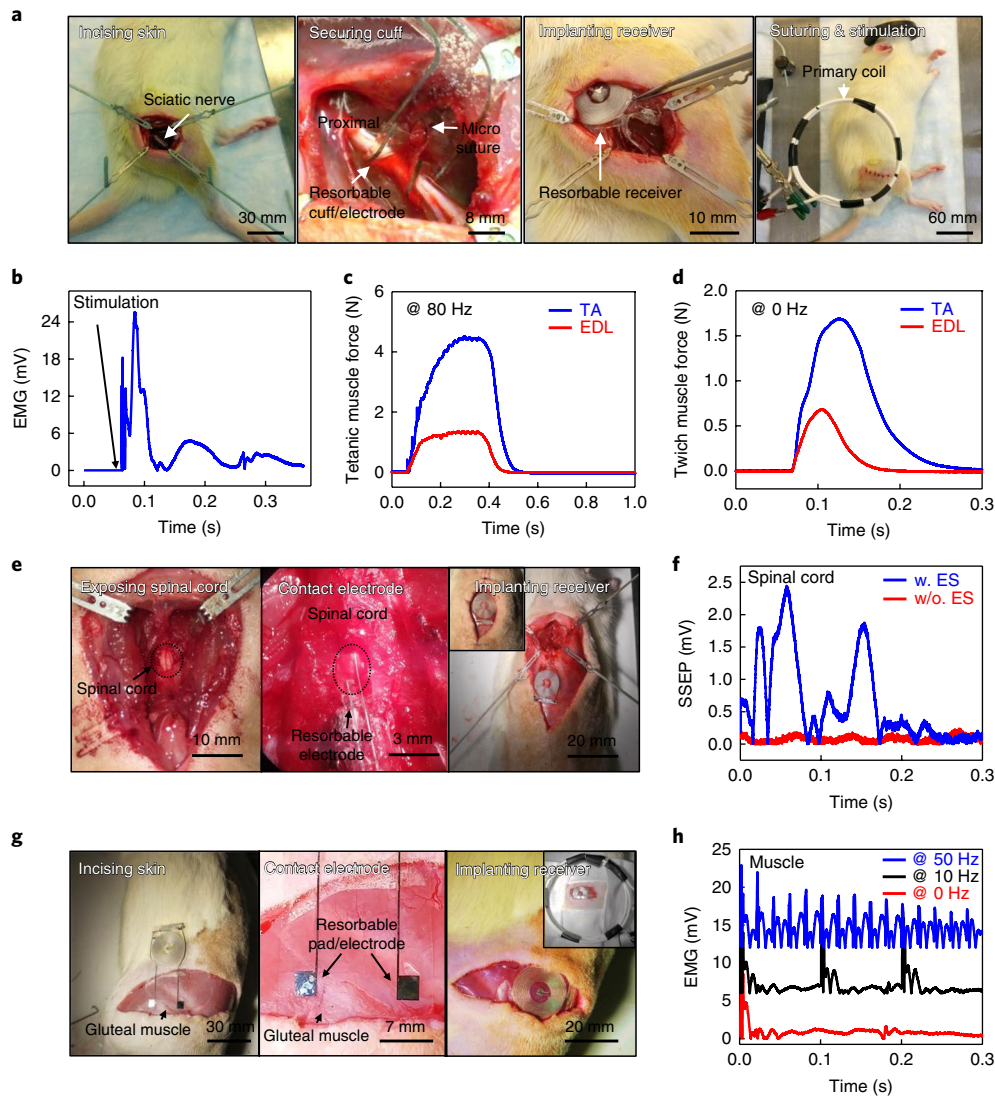


**Fig. 2 | Surgical implantation, operation, and acute demonstration of a bioresorbable, wireless electrical stimulator for the sciatic nerve in a rodent model.** **a**, Surgical procedure for implanting the device. From left to right: the skin is incised; the cuff is secured to the sciatic nerve with bioresorbable sutures (5-0 VICRYL); the radio frequency harvester unit is subcutaneously implanted to minimize movement; the skin is sutured and the stimulation is activated with a transmitting coil. **b**, EMG (rectified) signals measured at the tibialis anterior muscle while stimulating the sciatic nerve with a monophasic electrical waveform (200  $\mu$ s single pulse). Independent devices ( $n=10$ ) in independent animals ( $n=10$ ). **c,d**, Tetanic and twitch force at the tibialis anterior (blue) and EDL (red) muscles generated by monophasic stimulation at frequencies of 80 and 0 Hz, respectively. Independent devices ( $n=10$ ) in independent animals ( $n=10$ ). **e**, Picture of a bioresorbable stimulator designed for the spinal cord and image of the electrode/cord interface (inset image). **f**, Application in spinal cord stimulation. The flat, ribbon-shaped electrodes interface onto the surface of the spine. SSEP induced by electrical stimulation (monophasic, 10 Hz, 200  $\mu$ s per pulse) (red, without stimulation; blue, with stimulation). w. ES, with electrical stimulation; w/o. ES, without electrical stimulation. Independent devices ( $n=3$ ) in independent animals ( $n=3$ ). **g**, Picture of a bioresorbable stimulator designed for use with skeletal muscle and surgical image of implantation and operation. **h**, EMG measured during the stimulation of skeletal muscle at various frequencies (red, 0 Hz; black, 10 Hz; blue, 50 Hz). (A y axis offset of 10 and 15 mV for the data at 10 and 50 Hz, respectively, facilitates visual comparisons.) Independent devices ( $n=3$ ) in independent animals ( $n=3$ ).

also humans<sup>21</sup>; in both cases, the receiver unit could be placed just under the skin.

The unique defining characteristic of this system is that the constituent materials bioresorb in a controlled manner and within a defined time frame when exposed to biofluids found in and around subcutaneous tissue. Fig. 1g shows photographs of devices at various times following immersion in PBS at 37°C. Constituent materials dissolve within 3 weeks, while all remaining residues completely disappear after 25 d<sup>19,22,23</sup>. Ideally, bioresorption should commence shortly after the duration of bioelectrical therapy, adjusted by selecting the thicknesses and active

and passive materials (for example, PLGA, Candelilla wax<sup>24-26</sup>) (Supplementary Fig. 6).

Testing of nerve repair in animal models began with surgical implantation of the bioresorbable nerve stimulators through a dorsolateral gluteal-muscle-splitting incision used to expose the sciatic nerve, as shown in Fig. 2a. Wrapping the cuff around the nerve and securing the interface with a bioresorbable suture (6-0 Vicryl) forms a tubular electrode interface with excellent apposition to the nerve tissue. Inserting the harvester into a subcutaneous pocket created on the dorsolateral aspect of the hind limb and securing the harvester with bioresorbable sutures completes the implantation.

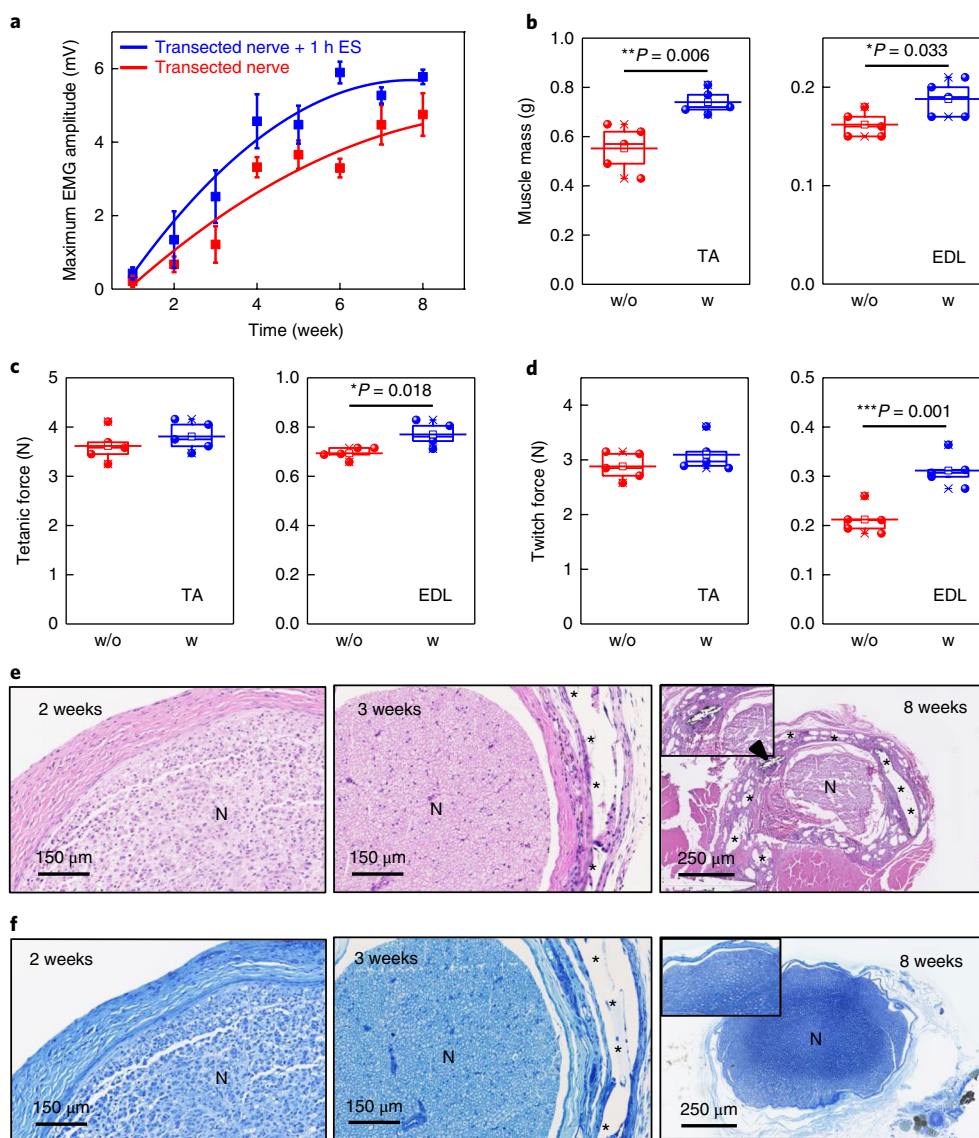


**Fig. 3 | Accelerated regeneration of sciatic nerves injured by transection, treated with the use of biodegradable wireless stimulators.** **a**, Maximum EMG amplitudes measured from the tibialis anterior muscle after transection/direct repair of the sciatic nerve. Here, 1h of monophasic stimulation (200  $\mu$ s pulse duration, 20Hz frequency, over minimum threshold voltage) (blue,  $n=11$  for 1–3 weeks and  $n=5$  for 4–8 weeks) relative to the control group (red,  $n=5$ ). Data are mean  $\pm$  s.e.m. **b**, Muscle mass measurements obtained at 8 weeks postoperatively following electrical stimulation in the tibialis anterior and EDL muscles ( $n=5$  independent animals). **c,d**, Evoked muscle force measurements obtained 8 weeks postoperatively in tibialis anterior and EDL muscles (w/o, without stimulation (red); w, with stimulation (blue);  $n=5$  independent animals). **e**, H&E-stained sections obtained at the interface between the metallic electrodes of the nerve cuff and the sciatic nerve. **f**, Toluidine blue-stained sections obtained at the interface between the metallic electrodes of the nerve cuff and the sciatic nerve. Black stars, residual PLGA substrate; black arrow, residual metallic lead; N, rat sciatic nerve.  $n=5$  independent animals. In **b–d**, The boxplots show the median (center line), the third and first quartiles (upper and lower edge of the box, respectively), and the largest and smallest value that is  $\leq 1.5$  times the interquartile range (the limits of the upper and lower whiskers, respectively). The Statistica software (version 6.0) was used for the statistical analysis followed by a *t*-test ( $*P < 0.05$ ,  $**P < 0.01$ ,  $***P < 0.001$ ).

Passing radio frequency power through a transmission antenna placed adjacent to the hind limb of the animal delivers electrical stimulation to the interfaced nerve, with a temporal pattern defined by modulation of power delivery to the antenna. Electromyograms (EMGs) obtained from the tibialis anterior muscle in uninjured animals confirm the ability of the device to stimulate the sciatic nerve at levels well above threshold. These values, as reported previously<sup>27</sup>, correspond to stimulation of all the nerve fibers via the electrodes placed around the target sciatic nerve. Fig. 2b shows data obtained on stimulation of the sciatic nerve with monophasic pulses. Measurements of the evoked muscle force provide additional means

for assessing the success of nerve recruitment. Fig. 2c,d summarize the evoked tetanic and twitch responses of the tibialis anterior and extensor digitorum longus (EDL) muscles elicited by a monophasic pulse at 80 and 0 Hz, respectively (details outlined in the Methods).

This bioresorbable platform can address a wide range of clinical scenarios and target tissues/organ systems, including the brain and spinal cord, skeletal muscles, and cardiac tissues with relatively few modifications to the form factor and interfacial electrode sites. Fig. 2e and Supplementary Fig. 7a show a system configured to interface to the spinal cord, with an image obtained following acute implantation. Fig. 2f and Supplementary Fig. 7b illustrate the

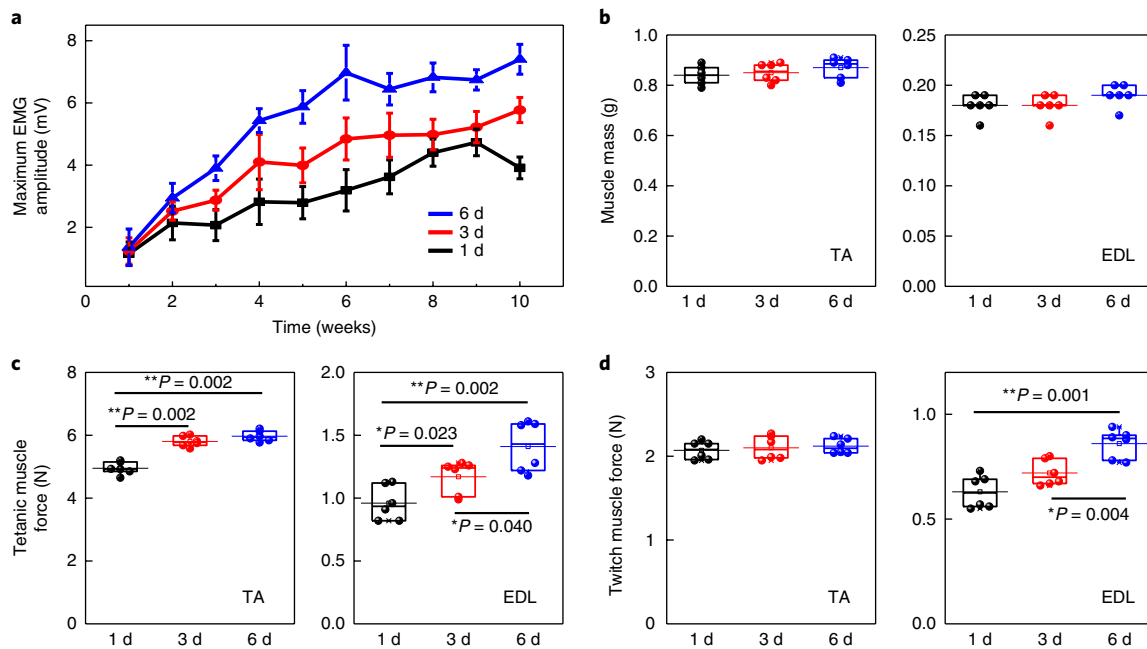


**Fig. 4 | Effects of chronic electrical stimulation on functional nerve recovery.** **a**, Time dependence of maximum EMG amplitude measured from tibialis anterior muscle after a transection injury of the sciatic nerve with electrical stimulation (200  $\mu$ s pulse, 20 Hz frequency, over a minimum threshold voltage) for 1 h per day for 1 d (black,  $n=6$  biologically independent animals), 3 d (red, data are mean  $\pm$  s.e.m.;  $n=6$  biologically independent animals), and 6 d (blue, data are mean  $\pm$  s.e.m.;  $n=6$  independent animals). **b**, Tibialis anterior and EDL muscle mass for three types of stimulation periods (1, 3, and 6 d). **c**, Evoked force of tibialis anterior and EDL muscle by extended periods of stimulation in tetanic muscle at 10 weeks. **d**, Evoked force of tibialis anterior and EDL muscle by extended periods of stimulation in twitch muscle at 10 weeks.  $n=6$  independent animals per stimulation condition (1, 3, 6 d). The boxplots show the median (center line), the third and first quartiles (upper and lower edges of the box, respectively), and the largest and smallest value that is  $\leq 1.5$  times the interquartile range (the limits of the upper and lower whiskers, respectively). The Statistica software (version 6.0) was used for the statistical analysis followed by a  $t$ -test (\* $P < 0.05$ , \*\* $P < 0.01$ , \*\*\* $P < 0.001$ ).

somatosensory evoked potential (SSEP) and motor evoked potential responses from stimulation of the spinal cord with monophasic pulses. Surgical images of the gluteal muscle in Fig. 2g demonstrate a device designed for muscle stimulation (Supplementary Fig. 7c). Fig. 2h presents the EMG response evoked from successful stimulation of the gluteal muscle with monophasic pulses at 0, 10, and 50 Hz, respectively.

Fig. 3 illustrates the capability of implantable wireless, bioresorbable stimulators to deliver the current standard of care (brief intraoperative electrical stimulation to injured nerve tissue), with equivalent outcomes of improved nerve regeneration and functional recovery as compared to existing nonresorbable nerve stimulators. Here, transecting the sciatic nerve with surgical scissors and performing a direct nerve repair establishes a reference for the time course and terminal degree of functional recovery without stimulation. In the experimental group, the same transection/repair injury was performed followed by application of direct electrical stimulation (Supplementary Fig. 8). Fig. 3a presents a series of EMG recordings from the tibialis anterior muscle at various stages after initial surgery for the groups with and without stimulation. Muscle activation in the tibialis anterior is greater in the presence of stimulation than in its absence for all stages of recovery, particularly 2–4 weeks postoperatively. Therapeutic electrical stimulation increases the rate of recovery during this time frame, such that muscle activation observed at 2 weeks postoperatively in the presence of electrical stimulation is equivalent to the results after 3 weeks in the absence of electrical stimulation. Similarly, muscle activation observed at 3 weeks postoperatively in the presence of electrical stimulation is equivalent to the results after 5 weeks in the absence of electrical stimulation. These results confirm that electrical stimulation delivered via bioresorbable stimulators is comparable in effect

and magnitude to electrical stimulation delivered by nonresorbable stimulators (Supplementary Fig. 9), both of which increase the rate of recovery compared to negative controls<sup>28</sup>.

Improvement in muscle activation during this critical stage of recovery suggests that electrical stimulation may support an increased rate of axonal regeneration and reduce the time to muscle reinnervation. Reduction in the total time of denervation positively affects both the time course and total quality of functional recovery in distal musculature. Terminal EMG amplitude increases to  $5.8 \pm 0.2$  mV in the presence of electrical stimulation from  $4.8 \pm 0.6$  mV in the absence of stimulation (Fig. 3a). Fig. 3b–d shows that tibialis anterior and EDL muscle mass improves in the presence of electrical stimulation after 8 weeks following the injury. The amplitude of evoked tetanic and twitch responses in tibialis anterior and EDL muscles also improves. Supplementary Fig. 10 shows a comparison of myelinated axons in normal nerve, injured nerve that did not receive electrical stimulation, and injured nerve that did receive electrical stimulation (1 h). Even at this relatively early time point, the observations confirm an increase in regenerating axons in the distal nerve site in the case of electrical stimulation. These findings support previous reports on axonal regeneration and recovery<sup>11,29–33</sup> and demonstrate the ability of bioresorbable stimulators to perform in a manner comparable to conventional, non resorbable implants.

H&E-stained sections obtained at the interface between the metallic electrodes of the nerve cuff and the sciatic nerve highlight the intact nature and close apposition of the bioresorbable substrate 8 weeks postimplantation in Fig. 3e. Minimal inflammatory response and fibrosis are observed in relation to the transient nerve cuff, and no evidence of axonal injury or damage is observed at the nerve/cuff interface. Fig. 3e shows that after 8 weeks in vivo, the

bioresorbable substrate is replaced by infiltrating macrophages, monocytes, lymphocytes, and fibroblasts, consistent with prior reports of the foreign body response to PLGA materials<sup>34,35</sup>. Metallic elements on the substrate also undergo dissolution and bioresorption at 8 weeks postimplantation (resorbing metallic lead indicated by the arrow in Fig. 3e at 8 weeks). As noted with PLGA nerve conduits of similar size and thickness to the present devices, residual particles of PLGA present before complete resorption do not elicit a cytotoxic response<sup>36,37</sup>. Fig. 3f reveals numerous healthy, myelinated axons in nerve fascicles directly adjacent to the bioresorbable substrate, metallic electrodes, and sites of electrical stimulation with no signs of inflammation or injury at either 3 or 8 weeks postimplantation. Previous studies of individual constituent materials used in the platforms presented here, such as PLGA<sup>34–38</sup>, Mg<sup>39</sup>, Mo<sup>40</sup>, Si nanomembranes<sup>22</sup>, and their use in other types of devices<sup>19</sup>, also provide strong evidence of biocompatibility.

The results summarized in Fig. 4 reveal that repeated 1-h daily applications of electrical stimulation during the early stages of recovery offer significant benefits in terms of the rate and degree of nerve regeneration and recovery of muscle function beyond the existing standard of care. Fig. 4a demonstrates enhanced therapeutic effects associated with multiple days of stimulation. At 10 weeks, tibialis anterior and EDL muscle mass improves with increasing duration of stimulation time (6 d), as shown in Fig. 4b. By comparison, stimulation for 1 and 3 d exhibits no appreciable change. Fig. 4c,d indicate that, as with other quantitative measures of recovery, evoked muscle force responses in tibialis anterior and EDL muscles (tetanic and twitch reactions) improve for the longest duration of electrical stimulation. Tetanic muscle force measurements (Fig. 4c) following 6 d of stimulation, compared with 1 d of stimulation, in tibialis anterior and EDL muscles improve by 1.02 N (*t*-test, *P*=0.002) and 0.45 N (*t*-test, *P*=0.002), respectively. Twitch muscle force measurements (Fig. 4d) following 6 d of stimulation, compared with 1 d of stimulation, in tibialis anterior and EDL muscles improve by 0.05 N (*t*-test, *P*=0.408) and 0.23 N (*t*-test, *P*=0.001), respectively.

Programmed electrical stimulation—up to 6 d beyond the intraoperative window—enabled by the use of wireless bioresorbable electronics represents an effective nonpharmacological adjunct useful in the management of critical nerve injuries. These findings establish the engineering foundations for broad classes of bioresorbable electronic implants that serve as functional conduits for applying neuroregenerative bioelectronic interventions across a range of clinical applications. Furthermore, these systems have broad applicability to a variety of targeted tissues and organ systems.

### Online content

Any methods, additional references, Nature Research reporting summaries, source data, statements of data availability and associated accession codes are available at <https://doi.org/10.1038/s41591-018-0196-2>.

Received: 16 January 2018; Accepted: 10 August 2018;

Published online: 8 October 2018

### References

- Noble, J., Munro, C. A., Prasad, V. S. & Midha, R. Analysis of upper and lower extremity peripheral nerve injuries in a population of patients with multiple injuries. *J. Trauma* **45**, 116–122 (1998).
- Kemp, S. W. P., Cederna, P. S. & Midha, R. Comparative outcome measures in peripheral regeneration studies. *Exp. Neurol.* **287**, 348–357 (2017).
- Sakiyama-Elbert, S. E. & Hubbell, J. A. Controlled release of nerve growth factor from a heparin-containing fibrin-based cell ingrowth matrix. *J. Control Release* **69**, 149–158 (2000).
- Sakiyama-Elbert, S. E. & Hubbell, J. A. Development of fibrin derivatives for controlled release of heparin-binding growth factors. *J. Control Release* **65**, 389–402 (2000).
- Taylor, S. J., McDonald, J. W. 3rd & Sakiyama-Elbert, S. E. Controlled release of neurotrophin-3 from fibrin gels for spinal cord injury. *J. Control Release* **98**, 281–294 (2004).
- Maxwell, D. J., Hicks, B. C., Parsons, S. & Sakiyama-Elbert, S. E. Development of rationally designed affinity-based drug delivery systems. *Acta Biomater.* **1**, 101–113 (2005).
- Wood, M. D. et al. Fibrin matrices with affinity-based delivery systems and neurotrophic factors promote functional nerve regeneration. *Biotechnol. Bioeng.* **106**, 970–979 (2010).
- Konofaos, P. & Terzis, J. K. FK506 and nerve regeneration: past, present, and future. *J. Reconstr. Microsurg.* **29**, 141–148 (2013).
- Labroo, P. et al. Controlled delivery of FK506 to improve nerve regeneration. *Shock* **46**, 154–159 (2016).
- Labroo, P., Shea, J., Sant, H., Gale, B. & Agarwal, J. Effect of combining FK506 and neurotrophins on neurite branching and elongation. *Muscle Nerve* **55**, 570–581 (2017).
- Gordon, T. Electrical stimulation to enhance axon regeneration after peripheral nerve injuries in animal models and humans. *Neurotherapeutics* **13**, 295–310 (2016).
- Nix, W. A. & Hopf, H. C. Electrical stimulation of regenerating nerve and its effect on motor recovery. *Brain Res.* **272**, 21–25 (1983).
- Ray, W. Z., Mahan, M. A., Guo, D., Guo, D. & Kliot, M. An update on addressing important peripheral nerve problems: challenges and potential solutions. *Acta Neurochir. (Wien)* **159**, 1765–1773 (2017).
- Cuoco, F. A. Jr & Durand, D. M. Measurement of external pressures generated by nerve cuff electrodes. *IEEE Trans. Rehabil. Eng.* **8**, 35–41 (2000).
- Leventhal, D. K., Cohen, M. & Durand, D. M. Chronic histological effects of the flat interface nerve electrode. *J. Neural Eng.* **3**, 102–113 (2006).
- Grill, W. M. & Mortimer, J. T. Neural and connective tissue response to long-term implantation of multiple contact nerve cuff electrodes. *J. Biomed. Mater. Res.* **50**, 215–226 (2000).
- Zierhofer, M. C. & Hochmair, E. S. Transcutaneous transmission of digital data and energy in a cochlear prosthesis system. *Int. J. Artif. Organs* **15**, 379–382 (1992).
- Winter, K. F., Hartmann, R. & Klinke, R. A stimulator with wireless power and signal transmission for implantation in animal experiments and other applications. *J. Neurosci. Methods* **79**, 79–85 (1998).
- Kang, S. K. et al. Bioresorbable silicon electronic sensors for the brain. *Nature* **530**, 71–76 (2016).
- Wodzicka, M. Studies on the thickness and chemical composition of the skin of sheep. *N.Z. J. Agric. Res.* **1**, 582–591 (1958).
- Fornage, B. D. & Deshayes, J. L. Ultrasound of normal skin. *J. Clin. Ultrasound* **14**, 619–622 (1986).
- Hwang, S. W. et al. Dissolution chemistry and biocompatibility of single-crystalline silicon nanomembranes and associated materials for transient electronics. *ACS Nano* **8**, 5843–5851 (2014).
- Yin, L. et al. Dissolvable metals for transient electronics. *Adv. Funct. Mater.* **24**, 645–658 (2014).
- Rojas-Molina, R., De León-Zapata, M. A., Saucedo-Pompa, S., Aguilar-Gonzalez, M. A. & Aguilar, C. N. Chemical and structural characterization of Candelilla (*Euphorbia antisiphilitica* Zucc.). *J. Med. Plant Res.* **7**, 702–705 (2013).
- Petersson, A. E. et al. Wax esters produced by solvent-free energy-efficient enzymatic synthesis and their applicability as wood coatings. *Green Chem.* **7**, 837–843 (2005).
- Vieira, M. G. A., da Silva, M. A., dos Santos, L. O. & Beppu, M. M. Natural-based plasticizers and biopolymer films: a review. *Eur. Polym. J.* **47**, 254–263 (2011).
- Gamble, P., Stephen, M., MacEwan, M. & Ray, W. Z. Serial assessment of functional recovery following nerve injury using implantable thin-film wireless nerve stimulators. *Muscle Nerve* **54**, 1114–1119 (2016).
- Brushart, T. M. et al. Electrical stimulation promotes motoneuron regeneration without increasing its speed or conditioning the neuron. *J. Neurosci.* **22**, 6631–6638 (2002).
- Elzinga, K. et al. Brief electrical stimulation improves nerve regeneration after delayed repair in Sprague Dawley rats. *Exp. Neurol.* **269**, 142–153 (2015).
- Gordon, T., Amirjani, N., Edwards, D. C. & Chan, K. M. Brief post-surgical electrical stimulation accelerates axon regeneration and muscle reinnervation without affecting the functional measures in carpal tunnel syndrome patients. *Exp. Neurol.* **223**, 192–202 (2010).
- Gordon, T. & English, A. W. Strategies to promote peripheral nerve regeneration: electrical stimulation and/or exercise. *Eur. J. Neurosci.* **43**, 336–350 (2016).
- Gordon, T., Udina, E., Verge, V. M. K. & de Chaves, E. I. P. Brief electrical stimulation accelerates axon regeneration in the peripheral nervous system and promotes sensory axon regeneration in the central nervous system. *Motor Control* **13**, 412–441 (2009).
- Willand, M. P., Nguyen, M. A., Borschel, G. H. & Gordon, T. Electrical stimulation to promote peripheral nerve regeneration. *Neurorehabil. Neural Repair* **30**, 490–496 (2016).

34. Christensen, M. B., Wark, H. A. C. & Hutchinson, D. T. A histological analysis of human median and ulnar nerves following implantation of Utah slanted electrode arrays. *Biomaterials* **77**, 235–242 (2016).
35. Srinivasan, A. et al. Microchannel-based regenerative scaffold for chronic peripheral nerve interfacing in amputees. *Biomaterials* **41**, 151–165 (2015).
36. Sasaki, R. et al. PLGA artificial nerve conduits with dental pulp cells promote facial nerve regeneration. *J. Tissue Eng. Regen. Med.* **5**, 823–830 (2011).
37. Yang, Y. et al. Biocompatibility evaluation of silk fibroin with peripheral nerve tissues and cells in vitro. *Biomaterials* **28**, 1643–1652 (2007).
38. Anderson, J. M. & Shive, M. S. Biodegradation and biocompatibility of PLA and PLGA microspheres. *Adv. Drug Deliv. Rev.* **64**, 72–82 (2012).
39. Gu, X., Zheng, Y., Cheng, Y., Zhong, S. & Xi, T. In vitro corrosion and biocompatibility of binary magnesium alloys. *Biomaterials* **30**, 484–498 (2009).
40. Lee, S. et al. Metal microparticle: polymer composites as printable, bio/coresorbable conductive inks. *Mater. Today* **21**, 207–215 (2018).

### Acknowledgements

S.-K.K. is supported by a National Research Foundation of Korea (NRF) grant funded by the Korean government (MSIT) (NRF-2018R1C1B5043901). H.M.L. is supported by a grant from NRF funded by the Korean government (MEST) (2011-0028612). Z.X. acknowledges support from the National Natural Science Foundation of China (grant no.11402134). Y.H. acknowledges support from National Science Foundation (grant nos. 1400169, 1534120, and 1635443). J.A.R. acknowledges support from DARPA and from the Center for Bio-Integrated Electronics at Northwestern University. We thank S. J. Robinson (Beckman Institute, University of Illinois at Urbana-Champaign) and K. Doty (Department of Comparative Biosciences Histology Service Laboratory,

University of Illinois at Urbana-Champaign) for histology staining and images that greatly improved the manuscript.

### Author contributions

J. Koo, S.-K.K., S.M.W., Y.-Y.C., S.C., and J.A.R. designed and made the device. J. Koo, M.R.M., S.-K.K., S.B.K., S.M.L., J. Kim, R.Z., J.S., D.V.H., A.B., H.M.L., W.Z.R., and J.A.R. conceived the idea and performed the experiments and analysis. M.R.M., M.S., P.G., N.B., J. Khalifeh, Z.S.Z., K.B., M.P., Y.Y., and W.Z.R. performed the animal surgery, collected the nerve regeneration data, and analyzed the immunohistochemistry. Z.X., K.L., B.J., and Y.H. designed the antennas and ran the electromagnetic simulation. J. Koo, S.-K.K., M.R.M., Y.H., W.Z.R., and J.A.R. wrote the manuscript.

### Competing interests

The authors declare no competing interests.

### Additional information

**Supplementary information** is available for this paper at <https://doi.org/10.1038/s41591-018-0196-2>.

**Reprints and permissions information** is available at [www.nature.com/reprints](http://www.nature.com/reprints).

**Correspondence and requests for materials** should be addressed to W.Z.R. or J.A.R.

**Publisher's note:** Springer Nature remains neutral with regard to jurisdictional claims in published maps and institutional affiliations.

© The Author(s), under exclusive licence to Springer Nature America, Inc. 2018

## Methods

### Preparation of bioresorbable components and assembly of wireless nerve stimulators.

A slab of poly(dimethylsiloxane) (PDMS, 9:1) served as a temporary substrate for a piece of Mg foil (~50 μm; Solution Materials) in a mixture of acetic acid and deionized water (1:10). Photolithography and wet etching in diluted hydrochloric acid (HCl:deionized water = 1:9) defined the radio frequency coil structures from this foil. The Mg radio frequency coil soaked with ethyl acetate (Sigma-Aldrich) was transferred onto a substrate of PLGA (65:35 (lactide:glycolide); Sigma-Aldrich) to yield the receiving antennas for radio frequency power harvesting. Depositing SiO<sub>2</sub> (~600 nm) on a piece of Mg foil patterned using the methods described earlier, laminating two such SiO<sub>2</sub>/Mg pieces together, face-to-face, and then embedding them in PLGA completed the manufacturing of the bioresorbable capacitor. Solid-state diffusion of boron (tube furnace at 1,000 °C with N<sub>2</sub> flow) and phosphorus (tube furnace at 1,050 °C with N<sub>2</sub> flow) through a photolithographically defined hard mask of SiO<sub>2</sub> formed by plasma-enhanced chemical vapor deposited yielded a PIN radio frequency diode with monocrystalline Si nanomembrane derived from an Si-on-insulator wafer (top silicon ~320 nm thick, *p* type; Soitec). Removing the buried oxide by immersion in hydrofluoric acid allowed release and transfer printing of the Si nanomembranes onto a sacrificial layer of diluted poly(pyromellitic dianhydride-co-4,4'-oxydianiline) (DPI; ~200 nm) on a film of poly(methyl methacrylate) (~300 nm) on a silicon wafer. Photolithographic patterning and reactive ion etching determined the lateral dimensions of the doped Si nanomembranes for integration into the diodes. Lift-off procedures applied with Mg deposited by electron beam evaporation (~300 nm thick; Kurt J. Lesker Company) defined the electrical contacts. Spin casting an overcoat of DPI and dry etching through the underlying DPI and poly(methyl methacrylate) to define an open mesh layout, followed by immersion in acetone, released the PIN diode and allowed its transfer to the PLGA substrate (~30 μm). Oxygen reactive ion etching removed the DPI layers during/after the transfer printing. Finally, these bioresorbable components (radio frequency coil, capacitance, PIN diode) were collected on a PLGA substrate. The individually transferred components were electrically interconnected with features of Mg deposited by sputtering (~2.5 μm) through a shadow mask. Coating the coils with PLGA and folding the system in half yielded a compact double-coil structure with openings for interconnections. Finally, laser-cutting the Mg foil (~50 μm thick) or Mo foil (10 μm thick) into 340-μm-wide electrodes and embedding them in PLGA yielded electrical wiring and interconnections to the cuff for the nerve interface.

**Electromagnetic simulation.** Finite element methods were adopted in electromagnetic simulations to determine the inductance, *Q* factor, and scattering parameters *S*<sub>11</sub> (matching with a 25 pF capacitor) of the bioresorbable, implantable wireless stimulator. The simulations were performed using the commercial software ANSYS HFSS (ANSYS), where the lumped port was used to obtain the scattering parameters *S*<sub>11</sub> (shown in Fig. 1d) and port impedance *Z*. An adaptive mesh (tetrahedron elements) was adopted to ensure computational accuracy. The inductance (*L*) and *Q* factor (*Q*) (shown in Supplementary Fig. 11c), were obtained from  $L = \text{Im}\{Z\}/(2\pi f)$  and  $Q = |\text{Im}\{Z\}/\text{Re}\{Z\}|$ , where  $\text{Re}\{Z\}$ ,  $\text{Im}\{Z\}$ , and *f* represent the real and imaginary parts of *Z*, and the working frequency, respectively. The self-resonance frequency *f*<sub>0</sub> = 6.5 MHz was then derived when *Q* = 0. To further evaluate the device performance, a transmission antenna (80 mm diameter, 3 turns) was added to obtain the relationship between the power transfer efficiency and working distance, as shown in Supplementary Fig. 11b.

**Experimental setup for the wireless stimulator.** Monophasic electrical impulses (duration: 200 μs; voltage: 200–500 mV<sub>pp</sub>) generated by a waveform generator (Agilent 33250A; Agilent Technologies) were amplified with a 201L amplifier (Electronics & Innovation). The resulting output was delivered to primary coils consisting of three turns of wire in an 80-mm-diameter loop (Alpha Wire 1560; Allied Electronics) with an adjustable matching capacitor (10–200 pF) (Supplementary Fig. 12). The receiver Mg coils had 17 turns of two layers (34 turns coil) in a 10-mm radius connected to an radio frequency diode and Mg/SiO<sub>2</sub>/Mg capacitor (10–50 pF). The received radio frequency power was transformed to a direct current output by this circuit. The direct current output voltage was measured with an oscilloscope connected to the Mg (Mo) cuff electrode (Supplementary Fig. 13d).

For the receiver oriented parallel to the transmitter in our system, the relationship between the distance *Z* (operating range) between the transmitter and receiver and the stimulator output voltage *V*<sub>0</sub> can be expressed as<sup>41</sup>

$$Z = \sqrt{\left(\frac{\pi\mu_0 N_T N_R S Q V_T a^2}{R V_0}\right)^{2/3} - a^2}$$

where  $\mu_0$  is the permeability of free space, *f* is the working frequency, *N*<sub>T</sub>, *R*, and *a* are the turn number, resistance, and radius of the transmission antenna, respectively, *N*<sub>R</sub>, *S*, and *Q* are the turn number, area, and quality factor of the loop antenna, respectively, and *V*<sub>T</sub> is the transmitting voltage. In our system, *f* is fixed at ~5 MHz to avoid the losses associated with absorption by biofluids. Therefore, for the fixed *a*,

and required output voltage *V*<sub>0</sub>, we need to increase *N*<sub>T</sub>, *N*<sub>R</sub>, *S*, *Q*, and *V*<sub>T</sub> but decrease *R* to improve the working range *Z*. Additional experiments appear in Supplementary Fig. 5. Here, chicken meat served as the medium for observing power transfer efficiency as a function of distance away from the primary antenna. Increasing the power to the primary antenna increases the output voltage at the stimulator.

**Therapeutic stimulation of injured nerve.** Animals underwent surgical transection and repair of the sciatic nerve 5 mm proximal to the trifurcation to evaluate the therapeutic effects of electrical stimulation delivered using the wireless, biodegradable devices. Following anesthetization, the sciatic nerve was transected using fine iris scissors and microsurgically repaired in a direct fashion using 10–0 nylon suture (SharpPoint™; Surgical Specialties Corporation). Immediately following nerve transection and repair, a biodegradable stimulator was implanted and interfaced to the sciatic nerve proximal to the site of coaptation. The surgical site was then closed as described earlier. Implanted stimulators were wirelessly activated to deliver therapeutic electrical stimulation (monophasic, 200 μs pulse, 20 Hz frequency, minimum amplitude over threshold) to the injured nerve for 1 h per day for 1, 3, or 6 consecutive days postoperatively.

**Monophasic and biphasic therapeutic stimulation.** In terms of the ability of monophasic and biphasic stimuli to recruit peripheral axons and induce axonal regeneration, prior studies have reported that the differences in waveform characteristic had a negligible effect<sup>42</sup>. In addition, there was no significant difference in pain threshold and tolerance between monophasic and asymmetric biphasic waveform<sup>43</sup>. Patel et al.<sup>44</sup> also reported that monophasic (pulsed direct current) stimulation evoked significant neurite outgrowth. Moreover, this growth is consistently oriented to the cathode<sup>44,45</sup>. Given these prior findings, and the limited duration of therapeutic electrical stimulation in the present study, monophasic, rather than biphasic, stimuli were used. Yet, modification of the transient electrical circuitry on the device enables generation of several biphasic waveforms, as shown in Supplementary Fig. 14. These results highlight the ability of the present device to support biphasic electrical stimuli suitable for use in future long-term *in vivo* studies. To that end, the authors believe that the fully resorbable nerve stimulator has immense flexibility of circuit design, and that the present dataset provides ample proof of the concepts of wireless interfacing and therapeutic electrical stimulation of injured nerve tissue.

**Functional lifetime of stimulator with PLGA or biodegradable wax encapsulation.** Mg radio frequency coils with PLGA encapsulation (30 μm) have operational lifetimes of 9 h *in vitro* (PBS at 37 °C, Supplementary Fig. 6). There, the addition of wax encapsulation can significantly extend the lifetime. Dip-coating in melted wax (Candelilla wax, ~70 °C) yielded a conformal film with a thickness of approximately 300 μm (Supplementary Fig. 6b). Soak testing in PBS at 37 °C for 14 d demonstrated stable operation throughout, due likely to the beneficial effects of the hydrocarbon chains of the wax as a water barrier<sup>24–26</sup>. Bioresorption of wax was slow compared with PLGA, from a few weeks to several months. To demonstrate functionality *in vivo*, encapsulated devices were implanted into male Lewis rats with the bioresorbable nerve cuff on the sciatic nerve. Implanted devices were then activated daily. Supplementary Fig. 6c provides a series of EMG recordings (10 Hz) from tibialis anterior muscles obtained from an uninjured animal to verify stable *in vivo* operation (200 μs, 100–300 mV, 1 h per day) for 1, 3, and 6 d, respectively. The maximum EMG amplitude, presented in Supplementary Fig. 6d, remains largely unchanged for 7 d. These results confirm the capability of bioresorbable nerve stimulators to successfully deliver multiple days of therapeutic electrical stimulation to injured nerve tissue.

**In vitro tests for longevity of the stimulator electrode.** Application of an electrical potential to metallic simulating electrodes causes accelerated dissolution by electrochemical reactions with surrounding fluids. Supplementary Fig. 15 shows the change of resistance of Mg (50 μm thick) and Mo (10 μm thick) metal wires in bovine serum at 37 °C. At high voltages (for example, 5 V), the Mg and Mo electrodes dissolved within 30 and 120 min, respectively. However, both types of electrodes were stable at 0.5 V (blue line) for up to 300 min, corresponding to 2 weeks of anticipated operating conditions (200 μs per pulse, 500 mV, 1 h per day). The therapeutic stimulation mode with the monophasic step pulses used in this study (200 μs per pulse, 20 Hz frequency, 1 h) corresponds to the application of a continuous potential for 15 min. The direct current resistance of the Mg electrode (50 μm thick) in bovine serum (37 °C) was increased 6, 7.5, 18.4, and 39.5 Ω for 5, 6, 7, and 8 d, respectively (Supplementary Fig. 15a). For long-term operation, Mo electrodes (10 μm thick) can be candidates because the impedance of Mo will not increase for up to 15 d (Supplementary Fig. 15b). Extended evaluations (Supplementary Fig. 15c,d) demonstrate that these wires survive for 6 d under the desired pulsed electrical stimulation (200 μs, 100–300 mV, 1 h per day). The design of durable nerve cuff interfaces and optimized procedures for surgical implantation, as described in the Supplementary Note, are also critical to achieving sufficient durations of electrical operation *in vivo*.

**Surgical procedures for bioresorbable electrodes designed to stimulate the spinal cord and muscle tissue.** Male Lewis rats (275–300 g, aged 10–11 weeks;

Charles River Laboratories) were anesthetized before undergoing a dorsal laminectomy at T10–T12 to evaluate the ability of bioresorbable electrodes to recruit spinal motor/sensory tracts in the spinal cord. Following surgical exposure, a bioresorbable electrode was inserted into the spinal canal rostral to the surgical site (T9–T9) such that the electrode was in contact with the dorsal surface of the spinal cord. Wireless activation resulted in delivery of monophasic pulses (duration: 200  $\mu$ s; threshold voltage: 100–300 mV) to the interfaced spinal tissue. Needle electrodes placed in the distal musculature of the right leg (tibialis anterior muscle) facilitated collection of motor evoked potential recordings. SSEP recordings were also collected using transcranial screw electrodes implanted over sensory cortical regions. Both motor evoked potential and SSEP recordings served to validate the ability of the bioresorbable device to electrically activate both sensory and motor spinal tracts postoperatively.

In the case of muscle stimulation, the right gluteal muscle was exposed following anesthesia and preparation of the lateral aspect of the right leg. A bioresorbable electrode placed on the surface of the gluteal muscle facilitated electrical stimulation of the interfaced muscle employing 0, 10, and 50 Hz monophasic pulses with a duration of 200  $\mu$ s. Needle electrodes placed into the gluteal muscle were used to record evoked EMGs within the muscle.

**Manufacturing of nonresorbable wireless nerve stimulators.** Implantable, nonresorbable wireless nerve stimulators were designed and built in collaboration with Red Rock Laboratories to provide a stable, low-profile, noninvasive means of facilitating chronic nerve stimulation<sup>27</sup>. The devices consisted of three components: (1) the receiver coil and demodulating circuit; (2) microwave leads; and (3) Si nerve cuff. Receiver coils comprising a spiral antenna and demodulating circuitry were constructed on flexible polyimide substrates (diameter = 12 mm, thickness = 0.2 mm) (Supplementary Fig. 8b); 0603 surface mount components were soldered to the flexible printed circuit board to tune the receivers to a 5 MHz carrier frequency and to demodulate incoming signals. Two multiconductor polytetrafluoroethylene-insulated Pt/Ir microwire leads (medwire; Sigmund Cohn Corp) were soldered on to the contact pads of the flexible polyimide printed circuit board to provide an electrical conduit between the receiver coil and interfaced peripheral nerves (Supplementary Fig. 8c). Bared ends of the Pt/Ir microwire leads were then integrated into Si nerve cuffs optimized for the rodent sciatic nerve (inner diameter = 2 mm, outer diameter = 4 mm, length = 8 mm). Si nerve cuffs were constructed of Si nerve guidance conduit and designed to maintain close approximation of the active Pt/It leads to interfaced peripheral nerve tissue. Following construction, flexible receiver coils were potted in medical grade Si elastomer (type A; Dow Corning). Completed wireless implants were gas-sterilized with ethylene oxide before use in vivo. On ex vivo/in vivo testing, modified class E oscillator circuits tuned to a 5 MHz carrier frequency were used to power and activate the constructed wireless nerve stimulators. Oscillator circuits were connected to circular transmitting coils/antenna placed near the wireless nerve stimulators. Inductive coupling between transmitter and receiver coils thereby facilitated wireless power delivery and activation of implantable wireless devices suitable for peripheral nerve stimulation.

**Therapeutic electrical stimulation of nerve tissue using permanent wireless stimulators following nerve crush and nerve transection injuries.** Twenty-five adult male Lewis rats (275–300 g, aged 10–11 weeks) were divided into five groups (I–V) of five animals each ( $n = 5$ ). Group I, the positive control, underwent sham surgical exposure of the right sciatic nerve (no nerve injury) followed by surgical implantation of a permanent wireless nerve stimulator. Groups II and IV, the experimental groups, underwent surgical exposure and either crush injury or transection injury of the right sciatic nerve, respectively, followed by surgical implantation of a permanent wireless nerve stimulator, yet no therapeutic electrical stimulation. Groups III and V, also experimental groups, underwent crush injury and transection injury of the right sciatic nerve, respectively, followed by surgical implantation of a permanent wireless nerve stimulator and 1 h of electrical stimulation delivered immediately postoperatively.

Weekly assessment of functional recovery was measured through electrical stimulation of the sciatic nerve by the non-bioresorbable nerve stimulator and measurement of resulting EMG signals in the distal musculature. Thirteen weeks postoperatively, animals from each group (I–V) were re-anesthetized before undergoing terminal assessment of functional nerve regeneration as measured via evoked muscle force measurement. At the terminal time point, all animals were killed and their distal musculature was harvested to measure wet muscle mass. All animal procedures were performed in strict accordance with the Animal Studies Committee and the Division of Comparative Medicine at Washington University School of Medicine.

Supplementary Fig. 16a–c summarize the outcomes of studies that use permanent nonresorbable wireless stimulators to deliver electrical stimulation (1 h at 20 Hz) to nerve tissue following nerve transection injury. These permanent platforms allow studies of EMG responses throughout the recovery period following 1 h of therapeutic stimulation delivered immediately postoperatively. Supplementary Fig. 16d–f show identical results on the delivery of therapeutic electrical stimulation to nerve tissue following nerve crush injury. Recovery of

muscle function is observed 2–4 weeks after injury in the presence of electrical stimulation, as the maximum EMG amplitudes of tibialis anterior, gastrocnemius, and plantaris muscles are significantly improved in the presence of electrical stimulation compared to responses in the absence of stimulation.

**Assessment of biocompatibility.** Rat sciatic nerve tissue and transient nerve cuffs were explanted and fixed in cold 3% glutaraldehyde in 0.1 M phosphate buffer (pH = 7.2). Nerve tissue was dissected and divided into segments, dehydrated in ethanol, postfixed with 1% osmium tetroxide, and embedded in Araldite 502 epoxy resin (Polysciences). Cross sections < 1  $\mu$ m thick were cut with an LKB III Ultramicrotome (LKB-Produkter AB) at the site of the nerve/cuff interface and stained with H&E and toluidine blue, respectively. Qualitative analysis was performed on H&E- and toluidine blue-stained sections using a semiautomated digital image analysis system, linked to software (LECO Corporation), as previously described<sup>46</sup>.

**Evoked muscle force measurement.** Thirteen weeks postoperatively, sciatic nerve function was terminally evaluated by examining force production in reinnervated musculature on electrical stimulation of the sciatic nerve. Following surgical exposure, distal tendons of the EDL and tibialis anterior muscles were fashioned into a loop and secured to a stainless steel S-hook at the musculotendinous junction using 5–0 nylon suture. Animals were subsequently placed in a designed functional assessment station (FAST System, version 2.0; Red Rock Laboratories) wherein the right leg was immobilized at the femoral condyles. The stainless steel S-hook was then connected to a 5 N thin-film load cell (S100; Strain Measurement Devices) supported on an adjustable mount. Cathodic, monophasic electrical impulses (duration = 200  $\mu$ s, frequency = single 200 Hz, amplitude = 0–5 mA) generated by implanted wireless nerve stimulators were delivered to the sciatic nerve proximal to the injury site. Resulting force production in the isolated EDL and tibialis anterior muscles was transduced via the load cell and recorded on a desktop PC equipped with data acquisition software (version 2.0; Red Rock Laboratories).

Evoked twitch responses were used to determine the optimal stimulus amplitude ( $V_o$ ) and optimal muscle length ( $L_o$ ) for isometric force production in the EDL muscle, as previously described<sup>47–49</sup>. On determining  $L_o$ , a single train of impulses (burst width = 300 ms, frequency = 80 Hz) was delivered to the sciatic nerve, and muscle length was reevaluated. All subsequent isometric force measurements were made at  $V_o$  and  $L_o$ . Single twitch contractions were recorded and peak twitch force ( $F_t$ ) was calculated. Tetanic contractions were recorded at increasing frequencies of stimulation (burst width = 300 ms, frequency = 5–200 Hz), allowing 2 min intervals between stimuli for muscle recovery. Maximum isometric tetanic force ( $F_o$ ) was automatically calculated from the resulting sets of recorded force traces. Following functional assessment, EDL and tibialis anterior muscles were harvested and weighed.

Evoked EMG responses were collected using Red Rock Laboratories data acquisition software (version 2.0) and analyzed using the MATLAB software, version 2009B (MathWorks). Supplementary Fig. 17 describes the conceptual procedure behind collecting the maximum EMG value. First, the instrumentation was calibrated. Second, raw EMG data were rectified to a single polarity. Then, the single maximum EMG peak was collected at each dataset. Finally, the maximum EMG values were averaged.

**Statistical analysis.** Results are reported as mean  $\pm$  s.d., unless otherwise noted. Statistical analyses were performed using the Statistica software (version 6.0; StatSoft) followed by a *t*-test (\* $P < 0.05$ , \*\* $P < 0.01$ , \*\*\* $P < 0.001$ ).

**Reporting Summary.** Further information on research design is available in the Nature Research Reporting Summary linked to this article.

## Data availability

The data that support the findings of this study are available from the corresponding author on reasonable request.

## References

- Lee, Y. *RFID Coil Design*. Report No. AN678 <http://ww1.microchip.com/downloads/en/AppNotes/00678b.pdf> (Microchip Technology Inc., 1998).
- Hingne, P. M. & Sluka, K. A. Differences in waveform characteristics have no effect on the anti-hyperalgesia produced by transcutaneous electrical nerve stimulation (TENS) in rats with joint inflammation. *J. Pain* **8**, 251–255 (2007).
- Barr, J. O., Nielsen, D. H. & Soderberg, G. L. Transcutaneous electrical nerve stimulation characteristics for altering pain perception. *Phys. Ther.* **66**, 1515–1521 (1986).
- Patel, N. B., Xie, Z., Young, S. H. & Poo, M. Response of nerve growth cone to focal electric currents. *J. Neurosci. Res.* **13**, 245–256 (1985).
- Winter, W. G., Schutt, R. C., Siskin, B. F. & Smith, S. D. Effects of low levels of direct current on peripheral nerve regeneration. *Trans. Orthop. Res. Soc.* **6**, 304 (1981).

46. Hunter, D. A. et al. Binary imaging analysis for comprehensive quantitative histomorphometry of peripheral nerve. *J. Neurosci. Methods* **166**, 116–124 (2007).
47. Mendez, J. & Keys, A. Density and composition of mammalian muscle. *Metabolism* **9**, 184–188 (1960).
48. Gans, C. Fiber architecture and muscle function. *Exerc. Sport Sci. Rev.* **10**, 160–207 (1982).
49. Kalliainen, L. K., Jejurikar, S. S., Liang, L. W., Urbanek, M. G. & Kuzon, W. M. Jr A specific force deficit exists in skeletal muscle after partial denervation. *Muscle Nerve* **25**, 31–38 (2002).

## Reporting Summary

Nature Research wishes to improve the reproducibility of the work that we publish. This form provides structure for consistency and transparency in reporting. For further information on Nature Research policies, see [Authors & Referees](#) and the [Editorial Policy Checklist](#).

### Statistical parameters

When statistical analyses are reported, confirm that the following items are present in the relevant location (e.g. figure legend, table legend, main text, or Methods section).

n/a Confirmed

- The exact sample size ( $n$ ) for each experimental group/condition, given as a discrete number and unit of measurement
- An indication of whether measurements were taken from distinct samples or whether the same sample was measured repeatedly
- The statistical test(s) used AND whether they are one- or two-sided  
*Only common tests should be described solely by name; describe more complex techniques in the Methods section.*
- A description of all covariates tested
- A description of any assumptions or corrections, such as tests of normality and adjustment for multiple comparisons
- A full description of the statistics including central tendency (e.g. means) or other basic estimates (e.g. regression coefficient) AND variation (e.g. standard deviation) or associated estimates of uncertainty (e.g. confidence intervals)
- For null hypothesis testing, the test statistic (e.g.  $F$ ,  $t$ ,  $r$ ) with confidence intervals, effect sizes, degrees of freedom and  $P$  value noted  
*Give  $P$  values as exact values whenever suitable.*
- For Bayesian analysis, information on the choice of priors and Markov chain Monte Carlo settings
- For hierarchical and complex designs, identification of the appropriate level for tests and full reporting of outcomes
- Estimates of effect sizes (e.g. Cohen's  $d$ , Pearson's  $r$ ), indicating how they were calculated
- Clearly defined error bars  
*State explicitly what error bars represent (e.g. SD, SE, CI)*

*Our web collection on [statistics for biologists](#) may be useful.*

### Software and code

Policy information about [availability of computer code](#)

Data collection

Evoked EMG and muscle force responses were collected using Red Rock Laboratories Data Acquisition Software (Red Rock Laboratories, Version 2.0, St. Louis, MO).

Data analysis

Evoked EMG and muscle force responses were analyzed using MATLAB software (MathWorks, Version 2009B, Natick, MA, USA). Statistical analyses were performed using Statistica software (Version 6.0, Statsoft, Tulsa, Oklahoma).

For manuscripts utilizing custom algorithms or software that are central to the research but not yet described in published literature, software must be made available to editors/reviewers upon request. We strongly encourage code deposition in a community repository (e.g. GitHub). See the Nature Research [guidelines for submitting code & software](#) for further information.

### Data

Policy information about [availability of data](#)

All manuscripts must include a [data availability statement](#). This statement should provide the following information, where applicable:

- Accession codes, unique identifiers, or web links for publicly available datasets
- A list of figures that have associated raw data
- A description of any restrictions on data availability

The authors declare that data supporting the findings of this study are available within the paper and its supplementary information files.

## Field-specific reporting

Please select the best fit for your research. If you are not sure, read the appropriate sections before making your selection.

Life sciences       Behavioural & social sciences       Ecological, evolutionary & environmental sciences

For a reference copy of the document with all sections, see [nature.com/authors/policies/ReportingSummary-flat.pdf](https://www.nature.com/authors/policies/ReportingSummary-flat.pdf)

## Life sciences study design

All studies must disclose on these points even when the disclosure is negative.

Sample size	Power analysis was performed to determine the minimum sample size for $\alpha = 0.05$ , with a two-tailed t-test and at a statistical power level of 80%, as utilized in prior studies [Gamble et al., 2016]. A minimum number of $n=5$ rats per group were utilized. For some key experiments, sample size was increased from $n=5$ rats per group to $n=11$ rats per group.
Data exclusions	No data points were excluded from analysis.
Replication	Experiments examining the efficacy of electrical stimulation in improving nerve regeneration and functional recovery were replicated in multiple groups of laboratory animals and multiple nerve injury models utilizing both permanent and bioresorbable nerve stimulators.
Randomization	All animals were randomized into experimental groups. Groups were counterbalanced for animal sex and group average body weight. Additional information is provided in the Online Methods section.
Blinding	All assessments of functional recovery (evoked muscle force, muscle mass, EMG amplitude, etc.) were performed in a blinded manner.

## Reporting for specific materials, systems and methods

### Materials & experimental systems

n/a	Involvement in the study
<input type="checkbox"/>	<input checked="" type="checkbox"/> Unique biological materials
<input checked="" type="checkbox"/>	<input type="checkbox"/> Antibodies
<input checked="" type="checkbox"/>	<input type="checkbox"/> Eukaryotic cell lines
<input checked="" type="checkbox"/>	<input type="checkbox"/> Palaeontology
<input checked="" type="checkbox"/>	<input type="checkbox"/> Animals and other organisms
<input checked="" type="checkbox"/>	<input type="checkbox"/> Human research participants

### Methods

n/a	Involvement in the study
<input checked="" type="checkbox"/>	<input type="checkbox"/> ChIP-seq
<input checked="" type="checkbox"/>	<input type="checkbox"/> Flow cytometry
<input checked="" type="checkbox"/>	<input type="checkbox"/> MRI-based neuroimaging

## Unique biological materials

Policy information about [availability of materials](#)

Obtaining unique materials	All the chemicals to fabricate biological polymers can be provided commercial bender (Sigma-Aldrich, Inc. USA). All the bio-metals (Mg, Mo) can be purchased through bender (Goodfellow Corporation, PA, USA).
----------------------------	--